An In Situ Simultaneous Reduction-Hydrolysis Technique for Fabrication of TiO_2-Graphene 2D Sandwich-Like Hybrid Nanosheets: Graphene-Promoted Selectivity of Photocatalytic-Driven Hydrogenation and Coupling of CO_2 into Methane and Ethane

Wenguang Tu, Yong Zhou, Qi Liu, Shicheng Yan, Shanshan Bao, Xiaoyong Wang, Min Xiao, and Zhigang Zou**

A novel, in situ simultaneous reduction-hydrolysis technique (SRH) is developed for fabrication of TiO_2--graphene hybrid nanosheets in a binary ethylenediamine (En)/H_2O solvent. The SRH technique is based on the mechanism of the simultaneous reduction of graphene oxide (GO) into graphene by En and the formation of TiO_2 nanoparticles through hydrolysis of titanium (IV) (ammonium lactato) dihydroxybis, subsequently in situ loading onto graphene through chemical bonds (Ti–O–C bond) to form 2D sandwich-like nanostructure. The dispersion of TiO_2 hinders the collapse and restacking of exfoliated sheets of graphene during reduction process. In contrast with prevenient G-TiO_2 nanocomposites, abundant Ti^{3+} is detected on the surface of TiO_2 of the present hybrid, caused by reducing agent En. The Ti^{3+} sites on the surface can serve as sites for trapping photogenerated electrons to prevent recombination of electron–hole pairs. The high photocatalytic activity of G-TiO_2 hybrid is confirmed by photocatalytic conversion of CO_2 to valuable hydrocarbons (CH_4 and C_2H_6) in the presence of water vapor. The synergistic effect of the surface-Ti^{3+} sites and graphene favors the generation of C_2H_6, and the yield of the C_2H_6 increases with the content of incorporated graphene. The work may open a new doorway for new significant application of graphene for selectively catalytic C–C coupling reaction

1. Introduction

CO_2 is a greenhouse gas of growing concern, and its atmospheric concentration continues to rise from the ongoing burning of fossil fuels. One of the best solutions is to convert CO_2 into valuable organic products by means of solar energy. Thus many research efforts have been made to develop efficient heterogeneous photocatalysts for the reduction of CO_2.[1–6] Considerable photocatalysts have been explored including semiconductors, such as TiO_2,[7–9] ZnO,[7,10] CdS,[7,11] $ZnGa_2O_4$,[12] Zn_2GeO_4,[13,14] and metal-incorporated metal–organic frameworks.[15] Coupling of co-catalysts such as platinum, Cu_xO and RuO_2 enhances stability of the photocatalysts against photocorrosion, improves a higher separation of photogenerated charge carriers, and increases the CO_2 conversion efficiency. Different products have been obtained over various photocatalysts under light illumination in presence of CO_2 and H_2O, such as CO, CH_4, CH_3OH, HCOOH or others.[5] Due to complex multielectron transfer process, however, the understanding of the catalytic selectivity and mechanism is in its infancy.[16–20]

Conversion C_1 species such as CH_4 to more valuable high-grade carbon species (C_n, $n \geq 2$, such as ethane, C_2H_6) under mild condition is a fundamental but significant transformation of great industrial importance, because the produced ethane can in turn be conveniently converted to liquid fuels or ethene through metathesis and dehydrogenation, respectively.[39] To

Dr. W. Tu, Prof. Y. Zhou, Dr. Q. Liu, Prof. Z. Zou
Eco-materials and Renewable Energy Research Center (ERERC)
Nanjing University
Nanjing 210093, P. R. China
E-mail: zhouyong1999@nju.edu.cn; zgzou@nju.edu.cn
Dr. W. Tu, Prof. Y. Zhou, Dr. S. Bao, Prof. X. Wang, Prof. M. Xiao, Prof. Z. Zou
School of Physics
Nanjing University
Nanjing 210093, P. R. China
Prof. Y. Zhou, Dr. S. Yan, Dr. S. Bao, Prof. X. Wang, Prof. M. Xiao, Prof. Z. Zou
National Laboratory of Solid State Microstructures
Nanjing University
Nanjing 210093, P. R. China
Dr. Q. Liu, Dr. S. Yan, Prof. Z. Zou
Department of Materials Science and Engineering
Nanjing University
Nanjing 210093, P. R. China

DOI: 10.1002/adfm.201202349

date, coupling of CH_4 into C_2H_6 by thermal routes for activation of the strong C–H bond (104 kcal mol^{-1}) requires high temperatures and multistep processes, and therefore they are energy-consuming and inefficient.[40] Compared to methods powered by thermal energy, techniques that use photonic energy to directly drive C–C coupling of CO_2 at room temperature undoubtedly have substantial advantages, such as the capacity to minimize coking.[41]

Graphene, a 2D honeycomb-like network of carbon atoms, has been used as a support for fabricating various nanohybrids with semiconductors, in which graphene is widely recognized to serve as an electron collector and transporter to efficiently hinder electron-hole recombination and lengthen the lifetime of the photo-generated charge carriers from semiconductor nanoparticles.[21] Besides those properties, exploring and advancing the graphene-relevant new performance is greatly important to expand the range of applications.[22] For instance, graphene can prevent CdS from photocorrosion during visible-light photocatalytic H_2 production.[23] Graphene is also able to promote CdS photocatalyst in selective oxidation of a range of alcohols to corresponding aldehydes under mild conditions.[24]

The conducting band of TiO_2 around –4.21 eV[37] and the work function of graphene of ≈4.42 eV[38] allow the charge transfer from TiO_2 to graphene. Thus, hybrid of graphene and TiO_2 (abbreviate as G-TiO_2) has drawn intense attention in the field of energy conversion and environmental applications.[21,25–36] We recently reported the preparation of robust G-$Ti_{0.91}O_2$ hollow spheres consisting of molecular-scale alternating titania nanosheets and graphene nanosheets as building blocks, which exhibit nine times increase of photocatalytic reduction of CO_2 into renewable fuels (CO and CH_4) relative to commercial P25[28] The large enhancement of the photocatalytic activity benefits from: 1) the ultrathin nature of $Ti_{0.91}O_2$ nanosheets allows charge carriers to move rapidly onto the surface to participate in the photoreduction reaction; 2) the sufficiently compact stacking of ultrathin $Ti_{0.91}O_2$ nanosheets with G nanosheets allows the photogenerated electron to fast transfer from $Ti_{0.91}O_2$ nanosheets to G to enhance lifetime of the charge carriers; and 3) the hollow structure potentially acts as a photon trap well to allow the multiscattering of incidence light for the enhancement of light absorption. Production of higher-level hydrocarbon fuel through CO_2 conversion will make such artificial photosynthesis more significant.

In this paper, we demonstrate a novel in situ simultaneous reduction-hydrolysis technique (SRH) for fabrication of 2D sandwich-like graphene-TiO_2 hybrid nanosheets in a binary ethylenediamine (En)/H_2O solvent. The so-called SRH technique is based on the mechanism of the simultaneous reduction of graphene oxide (GO) into graphene by En and the formation of TiO_2 nanoparticles through hydrolysis of titanium (IV) (ammonium lactato) dihydroxybis, subsequently in situ loading onto graphene through chemical bonds (Ti–O–C bond) to form 2D sandwich-like nanostructure. The dispersion of TiO_2 hinders the collapse and restacking of exfoliated sheets of graphene during reduction process. In contrast with prevenient G-TiO_2 nanocomposites, abundant Ti^{3+} was detected on the surface of TiO_2 of the present hybrid, caused by reducing agent En. The Ti^{3+} sites on the surface can serve as sites for trapping photogenerated electrons to prevent recombination of electron-hole pairs. The high photocatalytic activity of the G-TiO_2 hybrid was evaluated by photocatalytic conversion of CO_2 to valuable hydrocarbons (CH_4 and C_2H_6) in the presence of water vapor. The synergistic effect of the surface-Ti^{3+} sites and graphene favors the generation of C_2H_6, and the yield of the C_2H_6 increases with the content of incorporated graphene. Our work may open a new doorway for new significant application of graphene for selectively catalytic C–C coupling reaction.

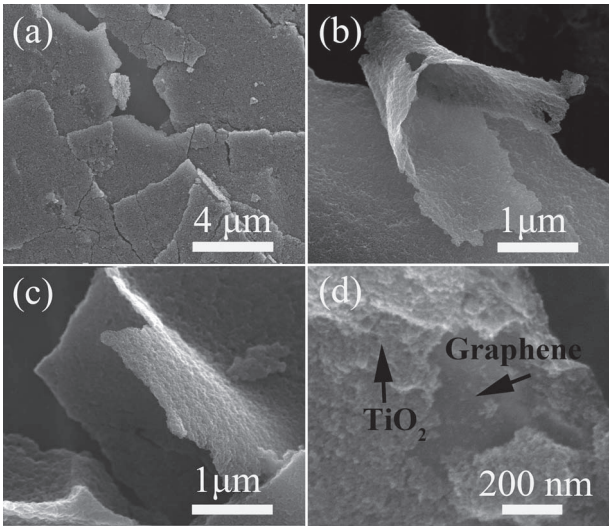

Figure 1. FE-SEM images of G2-TiO_2 at different magnifications.

2. Results and Discussion

G-TiO_2 composites with different weight percent of graphene were synthesized. The weight contents of graphene designated as x (wt%) in G-TiO_2 nanocomposites were 0, 1%, 2%, and 5%, and the corresponding samples were labeled as G0-TiO_2 (pure TiO_2), G1-TiO_2, G2-TiO_2, and G5-TiO_2 respectively. FE-SEM images (**Figure 1**) show that the typical G2-TiO_2 nanohybrid well maintains the 2D sheet-like structure of graphene with several-micrometer lateral size (Figure 1a) and exhibits remarkable structural flexibility (Figure 1b), which is in sharp contrast with irregular aggregation of the pure G0-TiO_2 nanoparticle formed in the absence of graphene (Supporting Information Figure S1). The TiO_2 nanoparticles with size of 10 to 20 nm of the hybrid are in intimate contact with graphene and uniformly distributed on the graphene nanosheets to form a sandwich-like structure (Figure 1c,d). A crack part of the hybrid clearly reveals the existence of graphene and TiO_2 nanoparticles, as indicated with arrowheads in the Figure 1d. It indicates that in situ loading of TiO_2 nanoparticles can not only be an effective way to prevent graphene nanosheets from being restacked during the reduction process, but also prevents the aggregation of TiO_2 nanoparticles.

TEM images (**Figure 2**) further reveal that a large number of TiO_2 nanoparticles spread uniformly and densely on the graphene. And the edge of the graphene can be clearly visible as indicated by the arrow (Figure 2b). No apparent aggregation of TiO_2 nanoparticles on the graphene further demonstrates that

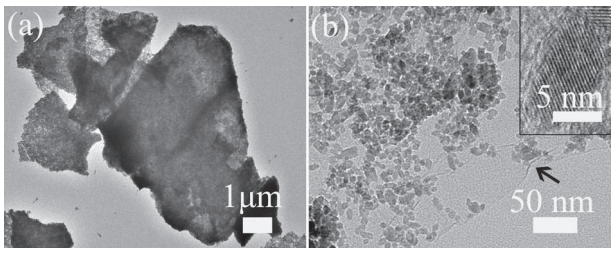

Figure 2. a,b) TEM images of G2-TiO_2. The inset of (b) shows high-resolution TEM image of G2-TiO_2.

graphene scaffold is able to spread the nanoparticles to hinder the aggregation. The high-resolution TEM image (the inset of Figure 2b) reveals well-defined lattice fringes of TiO_2 nanoparticle, corresponding to the (101) plane of anatase TiO_2.

Powder X-ray diffraction (XRD) patterns (Supporting Information Figure S2) show that all the identified peaks of G*x*-TiO_2 nanocomposites can be perfectly indexed to anatase TiO_2 (JCPDS card no. 21-1272).[29] With increasing graphene content, the diffraction peaks become weaker and the widths of the peaks become slightly wider, implying a slight decrease in the average crystallite size. The average crystallite size of TiO_2 determined by the (101) diffraction peak using the Scherrer equation slightly decrease from 15.3 nm to 12.8 nm (Supporting Information Table S1). It indicates that the graphene serve as a 2D "mat" well to anchor the forming TiO_2 nanoparticles to restrain from growing into large particles. No diffraction peak at about 25° assigned to the characteristic peak of restacked graphene appears, indicating that the regular stack was destroyed by the intercalation of TiO_2 particles.

As shown in Figure S3a (Supporting Information), the C1s XPS spectrum of as-used GO (solid line) clearly indicates a high degree of oxidation with three main components, corresponding to carbon atoms in different functional groups (dashed lines): C–C bond (284.6 eV), C–O/C=O bond (epoxy, hydroxyl and carbonyl) (286.7 eV), and O–C=O bond (carboxyl) (288.5 eV).[43,44] In the C1s XPS spectrum of the G2-TiO_2, the peak for C–O/C=O bond almost vanishes and the intensity of the peak for O–C=O band (dashed line) is much lower than that in GO, demonstrating the removal of most oxygen-containing functional groups. The C–C bond carbon content of G2-TiO_2 resumes drastically relative to GO (81% versus 46%), further confirming excellent restoration of the sp^2-hybridized carbon by the En-assisted solvothermal reduction process. The peak ascribed to Ti–C bond at around 281 eV is not detected in the spectrum of the G2-TiO_2, suggesting that Ti was not connected with carbon, and carbon was also not doped into the lattice of the TiO_2. In addition, appearance of a peak at 286.20 eV corresponding to C–N bond in the C1s XPS spectrum of G2-TiO_2[45] indicates that the reduction of GO is accompanied by nitrogen incorporation from the reducing agent En. A peak of amine group is also visible in the N1s XPS spectrum of G reduced by the solvothermal reduction process (Supporting Information Figure S4). The chemical state variations of Ti atoms on TiO_2 surface were studied through Ti2p XPS spectra of G-TiO_2 samples (Supporting Information Figure S3b). Two main peaks of pure TiO_2 located at 463.3 eV and 457.6 eV are assigned to Ti $2p_{1/2}$ and Ti $2p_{3/2}$, respectively. Compared to the Ti2p peak for Ti^{4+} (464.6 eV for Ti $2p_{1/2}$ and 458.9 eV for Ti $2p_{3/2}$), a shift of 1.3 eV toward the lower binding energy is visibly observed, indicating the formation of Ti^{3+}.[46] The Ti2p XPS spectrum of G2-TiO_2 also shows a shift of 1.1 eV. As the crystalline phase of the formed TiO_2 has no discernable change proved by XRD result, it is confirmed that Ti^{3+} was only formed on the surface of TiO_2. The reduction of Ti^{4+} to Ti^{3+} is possibly caused by reducing agent En. The Ti^{3+} sites on the surface can serve as sites for trapping photogenerated electrons to prevent recombination of electron-hole pairs.[47]

Fourier-transform infrared (FTIR) spectroscopic study shows the spectrum of GO and G2-TiO_2 (Supporting Information Figure S5). The characteristic absorption bands of GO[48] (1734 cm^{-1} for C=O stretching, 1240 cm^{-1} and 1370 cm^{-1} for C–OH stretching, 1077 cm^{-1} for C–O stretching) are absent, and in contrast the skeletal vibration at 1631 cm^{-1} attributed to the aromatic C=C group in G2-TiO_2 spectrum appears, suggesting that GO was primely reduced to graphene (Supporting Information Figure S5). The characteristic peak of En is not observed in the spectrum of G2-TiO_2, demonstrating that En is absent in the product.[49] Moreover, an obvious shoulder peak at around 798 cm^{-1} in the spectrum of G2-TiO_2 assigned to the Ti–O–C vibration was observed.[26] The results suggest that Ti atoms of TiO_2 can interact with the graphene to form chemisorption interfaces via Ti–O–C bonding. The presence of Ti–O–C band indicates that this method ensures good TiO_2–graphene contact through chemical bonds, favoring the charge transfer between TiO_2 and graphene upon light excitation. The Raman spectrum of G2-TiO_2 reveals the existence of two peaks of D band and G band of carbon species, indicating the existence of graphene, relative to G0-TiO_2 (Supporting Information Figure S6). The intensity ratio of the D band to G band, $I(D)/I(G)$, changes from 0.91 to 0.89, due to the removal of hydroxyl and epoxy groups, and the restoring of sp^2-hybridized carbon.

UV-visible (UV-vis) diffuse reflectance spectroscopy shows that G0-TiO_2 with an absorption edge at about 400 nm displays a bandgap of 3.1 eV (Supporting Information Figure S7). The absorption in the visible range is significantly enhanced as compared with pure TiO_2, which is attributed to the electronic interactions between the graphene and TiO_2,[26,31] and increases with increasing graphene ratio in G-TiO2, as evidence with the film color of the nanocomposites becoming darker (**Figure 3**).

To prove the favored impact of incorporated graphene on separation and transportation of photogenerated electron-hole

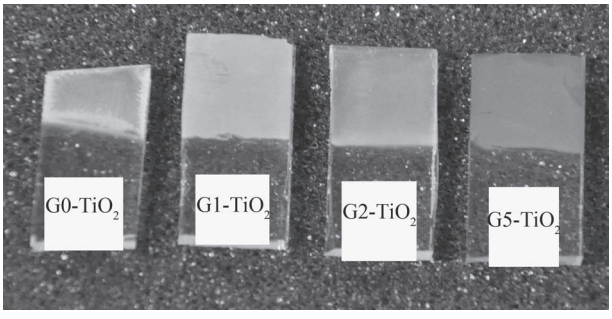

Figure 3. Photographs of samples G*x*-TiO_2 ($x = 0, 1, 2, 5$).

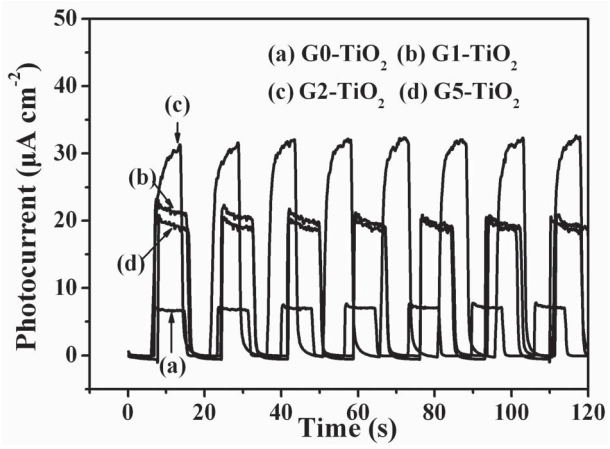

Figure 4. Photocurrent responses of samples G*x*-TiO_2 (*x* = 0, 1, 2, 5).

pairs under light irradiation, photocurrent measurements were carried out on G*x*-TiO_2 after deposition on FTO electrodes. **Figure 4** shows that the fast and reproducible photocurrent responses for each switch-on and switch-off light cycles for all G*x*-TiO_2 electrodes under UV light irradiation. With stopping of the illumination, the photocurrent decreases back to zero immediately. G*x*–TiO_2 photoanodes show significant enhancement in photocurrent response over TiO_2-only films. The enhancement of photocurrent demonstrates that photogenerated electrons in TiO_2 nanoparticles are transferred onto graphene and percolate to the collecting electrode, which is expected to minimize charge recombination losses. The photocurrents increase along with the increase of the mass ratio of GO from 1 to 2 wt%, reflecting the higher separation efficiency of photogenerated electron-hole pairs through electronic interaction between graphene and TiO_2. However, further increase of the mass ratio of GO (5 wt%) leads to a decrease of photocurrent intensity, probably due to intense light scattering and absorbance of the G.

The G0-TiO_2 exhibits a broad emission peak around 512 nm under bandgap excitation, arising from surface oxygen vacancies and surface defects of TiO_2 (**Figure 5**a).[50,51] The PL of these nanocrystals was suppressed after the hybridization with G, showing diminished PL intensity, which indicates reduced charge recombination in comparison to bare TiO_2. Under UV illumination, graphene accepts photogenerated electrons from TiO_2, resulting in the decrease of electron-hole recombination within TiO_2 and the PL quenching. This reduction increases with increasing graphene ratio in the G-TiO_2. Figure 5b compares TiO_2 emission decay traces as a function of increasing G concentration. The radiative lifetime of TiO_2 nanoparticles was obviously reduced when the graphene layers were incorporated. This also implies that an additional nonradiative decay channel through the transfer of electrons from TiO_2 to graphene is opened for the charge carriers created in the TiO_2 nanoparticles, consistent with PL quenching results.

The effect of graphene on the BET surface area and porous structure for G-TiO_2 samples was investigated using nitrogen adsorption-desorption measurements (Supporting Information Figure S8). The nitrogen adsorption-desorption isotherms of all samples are type IV, indicating the presence of mesopores.[52] For G0-TiO_2, a H1 hysteresis loops indicates agglomerates of uniform particles with high pore size uniformity and facile pore connectivity, proven by Figure S1 and the inset in Figure S8 (Supporting Information).[53] After hybridization of with graphene, the shape of the hysteresis loops of G2-TiO_2 and G5-TiO_2 is of type H3,[34] totally distinctly different from that of G0-TiO_2, which is associated with slit-like pores originating from stacking of the G-TiO_2 nanohybrid sheet. The pore size of mesopores ranges from 2 nm to 30 nm (inset in Supporting Information Figure S8). The porous structure of the G-TiO_2 facilitates the transportation of reactants and products through the interior space. The BET surface area (S_{BET}) of the nanohybrids gradually increases with increasing graphene content, from 95.8 to 114.9 m^2 g^{-1}, which is 1.8–2.1 times larger than that of P25. The amount of CO_2 absorbed on the G*x*-TiO_2 (*x* = 1, 2, 5) under ambient pressure at 0°C is 2–2.8 time larger than that of P25 and increases with increasing graphene content (Supporting Information Table S1).

To evaluate the photocatalytic activity of G-TiO_2 samples, the photocatalytic CO_2 conversion in the presence of water vapor was investigated. **Figure 6** shows that CO_2 can be photoreduced to CH_4 and C_2H_6 by using G-TiO_2 samples as photocatalysts

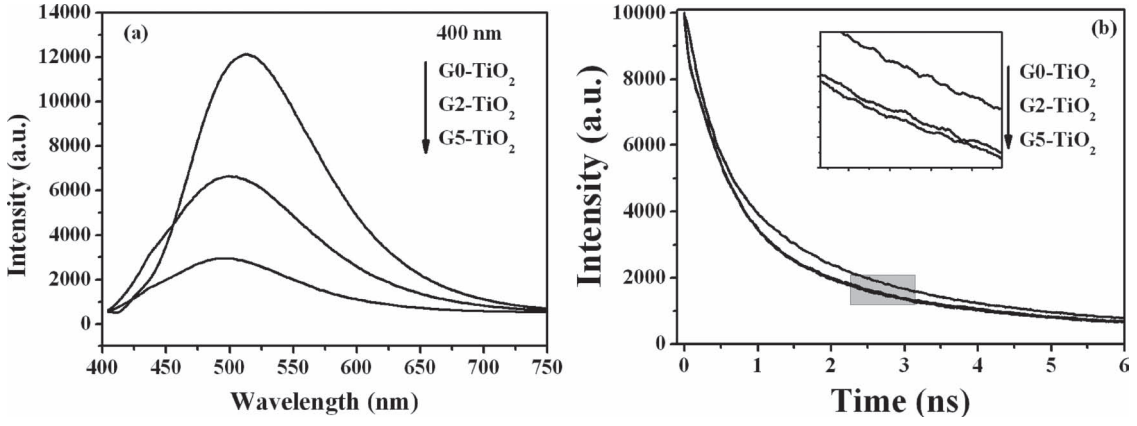

Figure 5. a) PL emission spectra and b) fluorescence decay traces of samples G*x*-TiO_2 (*x* = 0, 2, 5).

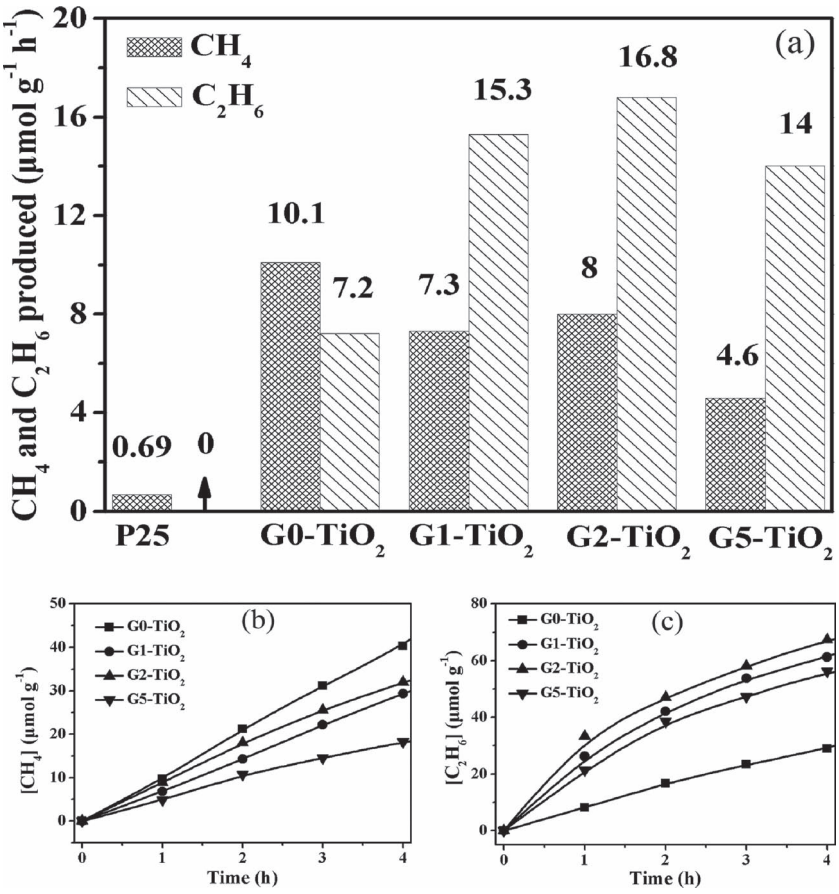

Figure 6. a) Comparison of photocatalytic activity of samples G*x*-TiO_2 (*x* = 0, 1, 2, 5) and P25. The molar ratio of C_2H_6 to CH_4 increases from 0.71 (for G0-TiO_2), 2.09 (G1-TiO_2), 2.10 (G2-TiO_2), to 3.04 (G5-TiO_2). b,c) Photocatalytic CH_4 and C_2H_6 evolution amounts for samples G*x*-TiO_2 (*x* = 0, 1, 2, 5).

without any noble-metal co-catalysts such as Pt and Au and oxides RuO_2. It is obvious that G0-TiO_2 (10.1 μmol g^{-1} h^{-1} CH_4 and 7.2 μmol g^{-1} h^{-1} C_2H_6) exhibits much higher activity than commercial P25 (0.69 μmol g^{-1} h^{-1} CH_4, and minor CO 0.16 μmol g^{-1} h^{-1}, C_2H_6 is absent).[28] The higher conversion is attributed to two factors: 1) the specific surface area of G0-TiO_2 is 2.73-time larger than that of commercial P25, offering more active adsorption sites and photocatalytic reaction centers; and 2) the surface of G0-TiO_2 has abundant Ti^{3+} sites which serves as energetically favorable sites for electron transfer to CO_2,[4,20] trapping electrons to prevent the recombination of electron-hole pairs. A CO_2 reduction experiment performed in the dark or in the absence of the photocatalysts showed no appearance of productions (CH_4 and C_2H_6), proving that the CO_2 reduction reaction is driven by light with the photocatalysts. With increasing graphene content, the total production rate increases. The enhanced conversion rate is attributed from that the d-orbital of TiO_2 and π-orbital of graphene match well in energy levels, and the G-TiO_2 have chemical bond interactions and form d–π electron orbital overlap. The excited-state electrons transporting from the TiO_2 upon UV illumination into the graphene can be shuttled freely along the conducting network of graphene, and subsequently transfer to the surface to react with CO_2, as schematically illustrated in **Figure 7**. The longer lifetime and mean free path for electrons on graphene implies that energetic electrons will cover a larger area of the graphene surface, thereby increasing the likelihood of interaction with adsorbed reactants. The total production rate reaches the highest value (8 μmol g^{-1} h^{-1} CH_4 and 16.8 μmol g^{-1} h^{-1} C_2H_6) with the graphene content of 2.0 wt%. However, a further increase of graphene content leads to a deterioration of photocatalytic performance, which may probably be attributed to increased scattering and absorbance of photons through excess graphene in the photocatalytic system, shielding the light from reaching the surface of TiO_2 photocatalysts. As a result, a suitable content of graphene is important for optimizing the photocatalytic activity of G-TiO_2 nanocomposites. With cooperation of graphene, an interesting phenomenon rises that the production rate of CH_4 slowly decreases but the production rate of C_2H_6 noticeably increases, i.e., the molar ratio of C_2H_6 to CH_4 increases from 0.71 (for G0-TiO_2), 2.09 (G1-TiO_2), 2.10 (G2-TiO_2), to 3.04 (G5-TiO_2), implying that C_2H_6 is easily produced with introduction of graphene. It is obvious that graphene has a right for selecting the products obtained by photocatalytic CO_2 conversion. Methoxyl ($^{\bullet}OCH_3$) and methyl ($^{\bullet}CH_3$) radicals were proved as reaction intermediates during the process of photocatalytic CO_2 conversion.[18,54–56] CH_4 can be produced by $^{\bullet}CH_3$ radical reacting with proton and electron ($^{\bullet}CH_3+H^+ + e^{-1} \rightarrow CH_4$) and coupling of two $^{\bullet}CH_3$ leads to C_2H_6 ($^{\bullet}CH_3+{}^{\bullet}CH_3 \rightarrow C_2H_6$).[57] Paul and Hoffmann[58] suggested that the dimerization of $^{\bullet}CH_3$ preferably occurs via a radical–substrate reaction mechanism in a hydrogen deficient system. The low coordinated oxygen species caused by abundant Ti^{3+} sites on the surface of TiO_2 generate relatively stronger active sites due to the suppression of acidic sites, thus the C_2 selectivity is more specific than that of the

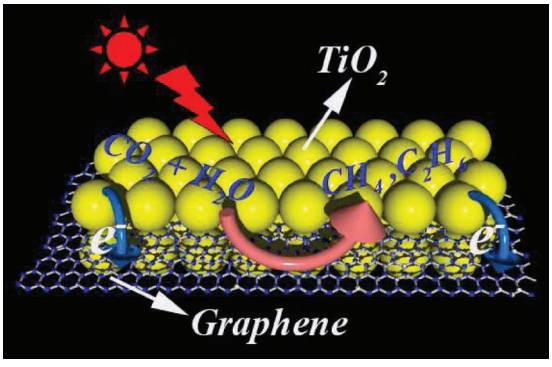

Figure 7. Schematic illustration of the charge separation and transfer in the G-TiO_2 system and photoreduction of CO_2 into CH_4 and C_2H_6.

higher acidic-based systems.[57] In the presence case, existence of abundance of Ti^{3+} sites on the surface through reduction of Ti^{4+} caused by reducing agent En plays vital role the coupling of photoformed $^{\bullet}CH_3$ radicals into C_2H_6 compared with commercial P25 and G-P25, which only produce CH_4.[21] For the G*x*-TiO_2 systems, $^{\bullet}CH_3$ radicals may be absorbed on the surface of graphene via π-conjugation between the unpaired electron of the radical and aromatic regions of the graphene.[26,27] The electron-rich graphene may help to stabilize the $^{\bullet}CH_3$ species, which restrains combination of $^{\bullet}CH_3$ with H^+ and e^{-1} into CH_4. Meanwhile, subsequent increasing accumulation of $^{\bullet}CH_3$ on the graphene raises the opportunity of formation of C_2H_6 by the coupling of $^{\bullet}CH_3$.

3. Conclusions

The so-called SRH technique was explored to fabricate 2D sandwich-like graphene-TiO_2 hybrid sheets. The dispersion of TiO_2 hinders the collapse and restacking of exfoliated sheets of graphene during reduction process. The photogenerated electrons in TiO_2 nanoparticles are transferred onto graphene under light irradiation, which minimizes charge recombination losses to improve the conversion efficiency of the photoreduction of CO_2 into hydrocarbon fuel. The synergistic effect of the surface-Ti^{3+} abundant TiO_2 and graphene favors the generation of C_2H_6, and the yield of the C_2H_6 increases with the content of incorporated graphene. Our work may open a new doorway for new significant application of graphene for selectively catalytic C–C coupling reaction.

4. Experimental Section

Materials: Titanium (IV) (ammonium lactato)dihydroxybis (50 wt% in aqueous solution) was purchased from Alfa Aesar. GO nanosheets were prepared using a modified Hummer's method from graphite powders.[42] Distilled water was used in all experiments.

Synthesis of G-TiO_2 Nanocomposites: G-TiO_2 nanocomposites with a varying amount of graphene were prepared by one-step hydrothermal method using GO nanosheets, En, and titanium (IV) (ammonium lactato)dihydroxybis as the starting materials. The synthesis procedure was as follows: a varying amount of GO, 1 g of titanium (IV) (ammonium lactato)dihydroxybis and 5 mL of En were dispersed into 10 mL of water and then stirred for 30 min at room temperature. The weight contents of graphene designated as *x* (wt%) in G-TiO_2 nanocomposites were 0%, 1%, 2%, and 5%, and the corresponding samples were labeled as pure TiO_2 (G0-TiO_2), G1-TiO_2, G2-TiO_2, and G5-TiO_2, respectively. Next, the mixtures were transferred into the stainless Teflon-lined autoclave of 25 mL inner volume, and then heated to 200 °C for 24 h under autogenous pressure, followed by cooling naturally to room temperature. The precipitates were collected by centrifugation, washed thoroughly with alcohol and water for three times respectively. Finally, the resulting products were dispersed in water by sonication and fully dried by lyophilization. For comparison, the bare graphene sample without any TiO_2 was prepared under the same experimental conditions and was labeled as G.

Characterization: The morphology of the samples was observed by the field emission scanning electron microscopy (FE-SEM) (FEI NOVA NanoSEM230, USA) and transmission electron microscopy (TEM) (JEOL 3010, Japan). The crystallographic phase of the as-prepared products was determined by powder X-ray diffraction (XRD) (Rigaku Ultima III, Japan) using Cu-Ka radiation (λ = 0.154178 nm) with scan rate of 10° min^{-1} at 40 kV and 40 mA. The crystallite size was calculated using Scherrer formula ($d = 0.9\lambda/B\cos\theta$, where d, λ, B and θ are crystallite size, Cu Kα wave length, full width at half maximum intensity (FWHM) in radians and Bragg's diffraction angle, respectively). The samples were analyzed with X-ray photoelectron spectroscopy (XPS) (K-Alpha, THERMO FISHERSCIENTIFIC). The XPS spectrum was calibrated with respect to the binding energy of the adventitious C1s peak at 284.8 eV. The specific surface area of the samples was measured by nitrogen sorption at 77 K on surface area and porosity analyzer (Micromeritics TriStar, USA) and calculated by the BET method. The CO_2 absorption on surface of the samples was evaluated by the above-mentioned adsorption apparatus under ambient pressure and 0 °C. Fourier transform infrared (FTIR) spectroscopy was conducted using a Nicolet NEXUS870 (USA) spectrometer. Raman spectra were measured on a JY HR800 laser Raman spectrometer (JOBIN YVON, France) with 488 nm argon laser excitation. The UV-visible (UV-vis) diffuse reflectance spectra were recorded with a UV-vis spectrophotometer (UV-2550, Shimadzu) at room temperature and transformed to the absorption spectra according to the Kubelka–Munk relationship.

Photocurrent Measurements: the photocatalysts were deposited on FTO electrode used as working electrodes by electrophoresis deposition method in the same condition. To attach photocatalysts to ITO glass, working electrodes were heated at 600 °C for 1 h in argon atmosphere. Photoelectrochemical measurements were carried out in a three-electrode configuration system: a FTO working electrode, Hg/Hg_2Cl_2 as the reference electrode, and a Pt foil as the counter electrode. Na_2SO_4 (1 M) aqueous solution was used as the electrolyte. The photocurrent was observed for each switch-on/off event by using a 500 W xenon lamp. The area of the samples exposed to light was 0.28 cm^2. An applied potential of working electrode against the counter electrode was set to 0.0 V.

Photocatalytic Experiments: In the photocatalytic reduction of CO_2, 0.1 g of samples was uniformly dispersed on the glass reactor with an area of 4.2 cm^2. A 300W Xenon arc lamp was used as the light source of photocatalytic reaction. The volume of reaction system was about 230 mL. The reaction setup was vacuum-treated several times, and then the high purity of CO_2 gas was followed into the reaction setup for reaching ambient pressure. 0.4 mL of deionized water was injected into the reaction system as reducer. The as-prepared photocatalysts were allowed to equilibrate in the CO_2/H_2O atmosphere for several hours to ensure that the adsorption of gas molecules was complete. During the irradiation, about 1 mL of gas was continually taken from the reaction cell at given time intervals for subsequent CH_4 or C_2H_6 concentration analysis by using a gas chromatograph (GC-2014, Shimadzu Corp., Japan). All samples were treated at 300 °C in nitrogen atmosphere for 2 h for removal of organic adsorbates before the photocatalysis reaction.

Supporting Information

Supporting Information is available from the Wiley Online Library or from the author.

Acknowledgements

This work was supported by 973 Programs (No. 2011CB933303, 2013CB632404, 2012CB921801, and 2011CBA00205), Fundamental Research Funds for the Central Universities (No. 1113020401, 1115020405 and 1116020406), NSFC (No. 20971048, 50732004, and 21173041), Jiangsu Provincial Funds for Distinguished Young Scientists (No. BK2012015) and Jiangsu Provincial Science and Technology Research Program (No. BK2011056).

Received: August 17, 2012
Published online: November 15, 2012

[1] H. Yoneyama, *Catal. Today* **1997**, *39*, 169.
[2] P. Usubharatana, D. McMartin, A. Veawab, P. Tontiwachwuthikul, *Ind. Eng. Chem. Res.* **2006**, *45*, 2558.
[3] G. R. Dey, *J. Nat. Gas Chem.* **2007**, *16*, 217.
[4] V. P. Indrakanti, J. D. Kubicki, H. H. Schobert, *Energy Environ. Sci.* **2009**, *2*, 745.
[5] S. C. Roy, O. K. Varghese, M. Paulose, C. A. Grimes, *ACS Nano* **2010**, *4*, 1259.
[6] M. R. Hoffmann, J. A. Moss, M. M. Baum, *Dalton Trans.* **2011**, *40*, 5151.
[7] T. Inoue, A. Fujishima, S. Konishi, K. Honda, *Nature* **1979**, *277*, 637.
[8] K. R. Thampi, J. Kiwi, M. Gratzel, *Nature* **1987**, *327*, 506.
[9] W.-N. Wang, W.-J. An, B. Ramalingam, S. Mukherjee, D. M. Niedzwiedzki, S. Gangopadhyay, P. Biswas, *J. Am. Chem. Soc.* **2012**.
[10] F. C. Meunier, *Angew. Chem. Int. Ed.* **2011**, *50*, 4053.
[11] Y. S. Chaudhary, T. W. Woolerton, C. S. Allen, J. H. Warner, E. Pierce, S. W. Ragsdale, F. A. Armstrong, *Chem. Commun.* **2012**, *48*, 58.
[12] S. C. Yan, S. X. Ouyang, J. Gao, M. Yang, J. Y. Feng, X. X. Fan, L. J. Wan, Z. S. Li, J. H. Ye, Y. Zhou, Z. G. Zou, *Angew. Chem. Int. Ed.* **2010**, *49*, 6400.
[13] Q. Liu, Y. Zhou, J. H. Kou, X. Y. Chen, Z. P. Tian, J. Gao, S. C. Yan, Z. G. Zou, *J. Am. Chem. Soc.* **2010**, *132*, 14385.
[14] N. Zhang, S. X. Ouyang, T. Kako, J. H. Ye, *Chem. Commun.* **2012**, *48*, 1269.
[15] Y. H. Fu, D. R. Sun, Y. J. Chen, R. K. Huang, Z. X. Ding, X. Z. Fu, Z. H. Li, *Angew. Chem. Int. Ed.* **2012**, *51*, 3364.
[16] S. Kaneco, H. Kurimoto, K. Ohta, T. Mizuno, A. Saji, *J. Photochem. Photobiol. A* **1997**, *109*, 59.
[17] M. Subrahmanyam, S. Kaneco, N. Alonso-Vante, *Appl. Catal. B-Environ.* **1999**, *23*, 169.
[18] C. C. Lo, C. H. Hung, C. S. Yuan, J. F. Wu, *Sol. Energy Mater Sol. Cells* **2007**, *91*, 1765.
[19] N. M. Dimitrijevic, B. K. Vijayan, O. G. Poluektov, T. Rajh, K. A. Gray, H. Y. He, P. Zapol, *J. Am. Chem. Soc.* **2011**, *133*, 3964.
[20] L. J. Liu, C.Y. Zhao, Y. Li, *J. Phys. Chem. C* **2012**, *116*, 7904.
[21] a) Y. T. Liang, B. K. Vijayan, K. A. Gray, M. C. Hersam, *Nano. Lett.* **2011**, *11*, 2865; b) Q. J. Xiang, J. G. Yu, M. Jaroniec, *Chem. Soc. Rev.* **2012**, *41*, 782.
[22] a) K. P. Loh, Q. L. Bao, G. Eda, M. Chhowalla, *Nat. Chem.* **2010**, *2*, 1015; b) K. P. Loh, Q. L. Bao, P. K. Ang, J. X. Yang, *J. Mater. Chem.* **2010**, *20*, 2277.
[23] L. Jia, D. H. Wang, Y. X. Huang, A. W. Xu, H. Q. Yu, *J. Phys. Chem. C* **2011**, *115*, 11466.
[24] N. Zhang, Y. H. Zhang, X. Y. Pan, X. Z. Fu, S. Q. Liu, Y. J. Xu, *J. Phys. Chem. C* **2011**, *115*, 23501.
[25] K. K. Manga, Y. Zhou, Y. L. Yan, K. P. Loh, *Adv. Funct. Mater.* **2009**, *19*, 3638.
[26] H. Zhang, X. J. Lv, Y. M. Li, Y. Wang, J. H. Li, *Acs Nano* **2009**, *4*, 380.
[27] J. C. Liu, H. W. Bai, Y. J. Wang, Z. Y. Liu, X. W. Zhang, D. D. Sun, *Adv. Funct. Mater.* **2010**, *20*, 4175.
[28] W.G. Tu, Y. Zhou, Q. Liu, Z. P. Tian, J. Gao, X. Y. Chen, H. T. Zhang, J. G. Liu, Z. G. Zou, *Adv. Funct. Mater.* **2012**, *22*, 1215.
[29] Y. H. Zhang, Z. R. Tang, X. Z. Fu, Y. J. Xu, *ACS Nano* **2011**, *5*, 7426.
[30] J. Du, X. Y. Lai, N. L. Yang, J. Zhai, D. Kisailus, F. B. Su, D. Wang, L. Jiang, *ACS Nano* **2010**, *5*, 590.
[31] J. S. Lee, K. H. You, C. B. Park, *Adv. Mater.* **2012**, *24*, 1084.
[32] C. Chen, W. M. Cai, M. C. Long, B. X. Zhou, Y. H. Wu, D. Y. Wu, Y. J. Feng, *ACS Nano* **2010**, *4*, 6425.
[33] N. Li, G. Liu, C. Zhen, F. Li, L. L. Zhang, H. M. Cheng, *Adv. Funct. Mater.* **2011**, *21*, 1717.
[34] S. B. Yang, X. L. Feng, K. Mullen, *Adv. Mater* **2011**, *23*, 3575.
[35] Q. J. Xiang, J. G. Yu, M. Jaroniec, *J. Am. Chem. Soc.* **2012**, *134*, 6575.
[36] H. I. Kim, G. H. Moon, D. Monllor-Satoca, Y. Park, W. Choi, *J. Phys. Chem. C* **2012**, *116*, 1535.
[37] Y. Xu, M. A. A. Schoonen, *Am. Mineral.* **2000**, *85*, 543.
[38] R. Czerw, B. Foley, D. Tekleab, A. Rubio, P. M. Ajayan, D. L. Carroll, *Phys. Rev. B* **2002**, *66*, 033408.
[39] S. F. A. Håkonsen, *Holmen in Handbook of Heterogeneous Catalysis*, vol. 7, (Eds: G. Ertl, H. Knözinger, F. Schüth, J. Weitkamp), Wiley-VCH, Weinheim **2008**, pp. 3384–3400.
[40] H. D. Gesser, N. R. Hunter, C. B. Prakash, *Chem. Rev* **1985**, *85*, 235.
[41] L. Li, G. D. Li, C. Yan, X. Y. Mu, X. L. Pan, X. X. Zou, K. X. Wang, J. S. Chen, *Angew. Chem. Int. Ed.* **2011**, *50*, 8299.
[42] L. J. Cote, F. Kim, J. X. Huang, *J. Am. Chem. Soc.* **2009**, *131*, 1043.
[43] J. I. Paredes, S. Villar-Rodil, P. Solís-Fernández, A. Martiínez-Alonso, J. M. D. Tascőn, *Langmuir* **2009**, *25*, 5957.
[44] R. S. Dey, S. Hajra, R. K. Sahu, C. R. Raj, M. K. Panigrahi, *Chem. Commun.* **2012**, *48*, 1787.
[45] J. F. Che, L. Y. Shen, Y. H. Xiao, *J. Mater. Chem* **2010**, *20*, 1722.
[46] P. Sangpour, F. Hashemi, A. Z. Moshfegh, *J. Phys. Chem. C* **2010**, *114*, 13955.
[47] K. Suriye, P. Praserthdam, B. Jongsomjit, *Appl. Surf. Sci.* **2007**, *253*, 3849.
[48] Z. Y. Huang, H. H. Zhou, C. H. Li, F. Y. Zeng, C. P. Fu, Y. F. Kuang, *J. Mater. Chem.* **2012**, *22*, 1781.
[49] Z. X. Deng, C. Wang, M. X. Sun, Y. D. Li, *Inorg. Chem* **2002**, *41*, 869.
[50] Y. Yao, G. Li, S. Ciston, R. M. Lueptow, K. A. Gray, *Environ. Sci. Technol.* **2008**, *42*, 4952.
[51] N. D. Abazovic, M. I. Comor, M. D. Dramicanin, D. J. Jovanovic, S. P. Ahrenkiel, J. M. Nedeljkovic, *J. Phys. Chem. B* **2006**, *110*, 25366.
[52] K. S. W. Sing, D. H. Everett, R. Haul, L. Moscou, R. A. Pierotti, J. Rouquerol, T. Siemieniewska, *Pure Appl. Chem.* **1985**, *57*, 603.
[53] M. Kruk, M. Jaroniec, *Chem. Mater.* **2001**, *13*, 3169.
[54] N.M. Dimitrijevic, B. K. Vijayan, O. G. Poluektov, T. Rajh, K. A. Gray, H. He, P. Zapol, *J. Am. Chem. Soc.* **2011**, *133*, 3964.
[55] M. Anpo, H. Yamashita, Y. Ichihashi, S. Ehara, *J. Electroanal. Chem.* **1995**, 21.
[56] H. Yamashita, H. Nishiguchi, N. Kamada, M. Anpo, *Res. Chem. Intermed.* **1994**, *20*, 815.
[57] M. Subrahmanyam, S. Kaneco, N. Alonso-Vante, *Appl. Catal. B-Environ.* **1999**, *23*, 169.
[58] J. Paul, F. M. Hoffmann, *Catal. Lett.* **1988**, *1*, 445.